2024 IEEE International Conference on Robotics and Automation (ICRA 2024)
May 13-17, 2024. Yokohama, Japan

Task-space Control of a Powered Ankle Prosthesis

David J. Kelly, Ryan R. Posh, and Patrick M. Wensing

***Abstract*— Powered lower-limb prostheses have shown promise in helping individuals with amputation regain functionality that passive prostheses cannot provide. However, the best method for controlling these devices in coordination with their users is still an open research topic. While powered devices can replicate normative joint kinematics and kinetics, active control also holds the potential to shape system-level characteristics such as the center of mass (CoM) that play an important role in balance. Controlling the prosthesis based on these system-level, or task-space, variables would further represent a new way of coordinating the user and their device.**

This paper explores the initial implementation of task-space control for a powered ankle prosthesis, characterizing the emergent outcomes of this new coordination strategy. One able-bodied subject walked using a bypass adapter while prosthesis torques were commanded based on reference ground reaction force (GRF) and CoM trajectories. The subject could walk comfortably and continuously at their preferred walking speed, achieving normative ankle torques and joint trajectories despite not tracking explicit joint-level references in stance.

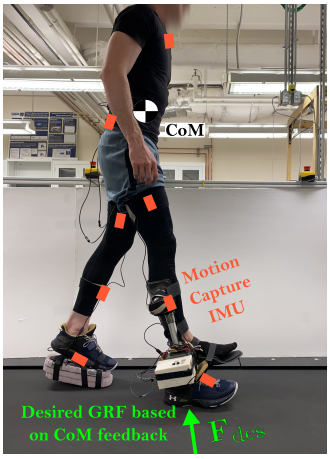

Fig. 1. An able-bodied subject walking on the Open Source Leg (OSL) using a bypass adapter while wearing an XSENS motion capture suit. CoM kinematics are incorporated via feedback during the stance phase.

I. Introduction

Walking is a daily activity that requires coordinated weight transfer between legs to maintain balance. This coordination is significantly impacted by lower-limb amputation, with prosthesis users seeing a much higher incidence of falls [1]. While passive prostheses remain the standard of care, recent research has shown major strides in the performance and reliability of powered devices [2]. Many excellent designs have emerged to reduce the size and weight of these devices [3], [4], such that a major barrier to their progress is finding ways to control the device in coordination with the user. Two methods of control have been implemented with high levels of success, namely position and impedance control.

Position control focuses on matching a reference trajectory through high-gain feedback [5], [6]. High-fidelity joint angle tracking requires high stiffness to avoid oscillations, which can feel unnatural to the user [7]. Impedance control instead focuses on rendering tunable stiffness, damping, and equilibrium characteristics [8], [9] via control of the joint torque. This method may feel more natural to the user, however, it can require tedious parameter tuning when used in a finite state machine (FSM) [7].

Using sensing that is isolated to the device itself or to the lower limbs, these methods of control demonstrate the ability to generate normative kinematic/kinetic joint profiles [8]. Furthermore, robustness to perturbations based on lower-limb neuromuscular models [10] and intuitive obstacle avoidance via monitoring of the residual thigh during swing [11] have helped address stability concerns during powered prosthesis use. These improvements in functionality can help build trust between a user and their device. Further synergy between user and device may be accomplished by expanding the information available to the controller with sensing beyond the lower limbs. By viewing the user and device as a system, rather than two separate entities, control may be developed from a goal- or task-level perspective.

Arguably the most important task-level quantity for walking and balance is the Center of Mass (CoM). Previous research suggested that foot placement strategies during walking may be influenced by how the CoM position [12] and the combination of CoM position and velocity [12], [13] interact with the base of support to maintain balance. Other work has found that muscle activity during balance recovery is more accurately reconstructed from CoM kinematic feedback as opposed to joint-level feedback [14], suggesting that task-level variables may guide whole-body coordination in able-bodied individuals. Control focused on the CoM has also been important in the development of walking robots, where reduced-order CoM models such as the linear inverted pendulum (LIP) and Bipedal Spring-Loaded Inverted Pendulum (B-SLIP) have been used for gait design and stabilization (e.g., [15]–[17]) with associated capture points [18] playing a role in push-recovery controllers. The importance of the CoM for the stability of bipedal locomotion encourages its incorporation in the control of lower-limb prostheses (Fig. 1).

The primary contribution of this paper is the introduction

*This work was funded by the National Science Foundation Award CMMI-1943703

*All authors are with the Department of Aerospace and Mechanical Engineering, University of Notre Dame, 365 Fitzpatrick Hall of Engineering, Notre Dame, Indiana dkelly@nd.edu

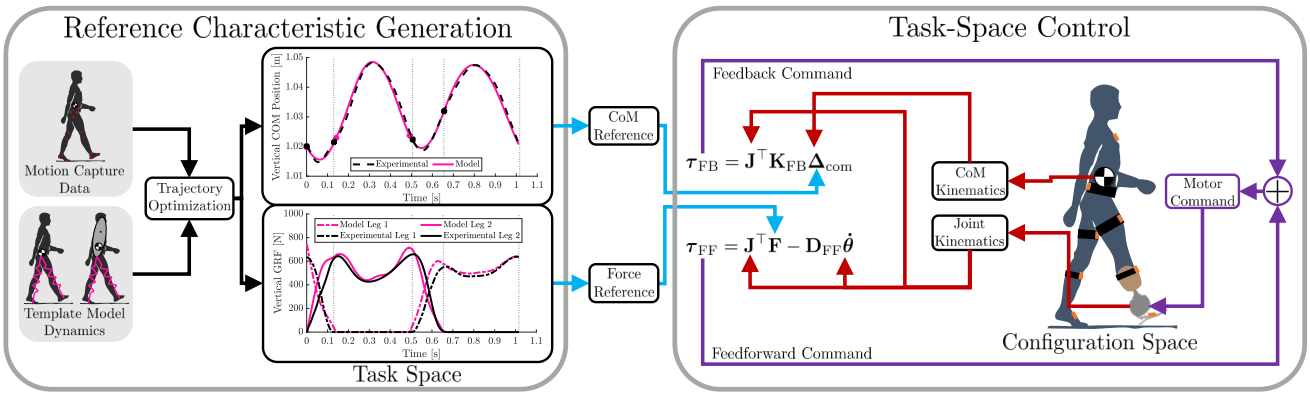

Fig. 2. Task-space control architecture for lower-limb prostheses.

of a control framework for lower-limb prostheses that incorporates reference CoM kinematics and ground reaction forces (GRFs) as inputs, herein called Task-space Control (TSC). Explicitly including task-space variables like the CoM into the control coordinates the user and their prosthesis at a system level, which may promote increased synergy between user and device. We focus first on an ankle-only prosthesis to develop the main ideas of this approach. Despite the new focus on task-level variables, we show that the resulting gait retains normative joint kinematics and kinetics.

II. Control Architecture

A. System Overview

The control framework presented here (Fig. 2) has two primary components. The left side of Fig. 2 corresponds to offline task-space reference generation. Reference CoM and GRF trajectories are used to determine joint torques online. Creating these task-space trajectories is detailed in Sec. II-B.

The right side of Fig. 2 highlights the use of the task-space references with real-time CoM, segment, and joint kinematic data to determine the actuator joint torques. The reference GRFs are combined with the joint kinematics for the feedforward joint torque, while the reference CoM kinematics are used with the CoM information for feedback control. These torque calculations are detailed in Sec. II-C.

To ensure appropriate actuation across the gait cycle, progression is monitored using a phase variable based on the tibia kinematics [19], [20], as described in Sec. II-D. This phase variable is used to coordinate the progression through the reference CoM/GRF profiles and to appropriately switch between the stance and swing controller.

B. Reference Characteristic Generation

Following amputation and the prescription of a standard-of-care device, gait characteristics such as vertical CoM displacement and vertical GRF are often negatively impacted [21], [22]. This outcome has motivated past controllers for active prostheses (e.g., [9]) to employ normative reference data. For ankle prostheses, it is common to track reference trajectories for the ankle angle/torque. This approach has been successfully implemented due in part to the fact that joint torques (scaled by weight) and joint kinematics (used directly) generally show agreement across individuals [23]. However, for the CoM, additional normalizing factors need to be considered. We develop those here to ultimately adapt CoM reference trajectories from able-bodied users to new users with different heights and weights.

To generate reference profiles, a data set of 24 young healthy individuals walking at their preferred walking speed (PWS) was used [24]. Lower extremity motion capture data was used to estimate the horizontal and vertical CoM kinematics, with force plate data used to segment the CoM data into gait cycles.

For each individual, CoM kinematics were averaged over the gait cycle, defined by successive heel strikes of a particular foot. The horizontal and vertical CoM positions (x, z) were then normalized for each user at each instant j of the gait cycle using

$$\bar{x}_j = \frac{(x_j - T_j v)\sqrt{\ell_0 g}}{v} \qquad \bar{z}_j = \frac{z_j - z_{\text{avg}}}{H} \tag{1}$$

where $\bar{x}$ and $\bar{z}$ are the scaled horizontal/vertical CoM position, T is a time parameter that increases from 0 to the average stride time as j increases, v is the average walking speed, ℓ_0 is the measured leg length, g is gravity, z_{avg} is the average vertical CoM height, and H is the measured height of the user. The scaled CoM kinematics for all 24 individuals in the dataset were then combined and averaged.

The desired CoM kinematics (x^*, z^*) for a new user were calculated by rearranging Equation 1 as

$$x_j^* = \frac{\bar{x}_j v}{\sqrt{\ell_0 g}} + T_j v \qquad z_j^* = H \bar{z}_j + z_{\text{avg}}. \tag{2}$$

using new parameters H, v, and z_{avg} for the new subject, with v and z_{avg} based on a single walking trial with the prosthesis operating passively.

To transform these samples into a smooth physically feasible reference, the resulting (x^*, z^*) were fit to the Bipedal Spring-Loaded Inverted Pendulum (B-SLIP) template model of walking using the methods described in [25]. The optimization provides highly accurate CoM kinematics (<1 cm RMSE), as well as GRF and stiffness profiles with respect to the percentage of gait cycle. The CoM kinematics and GRF profiles for the implementation in this paper are illustrated in Fig. 3. The stiffness profiles of the B-SLIP

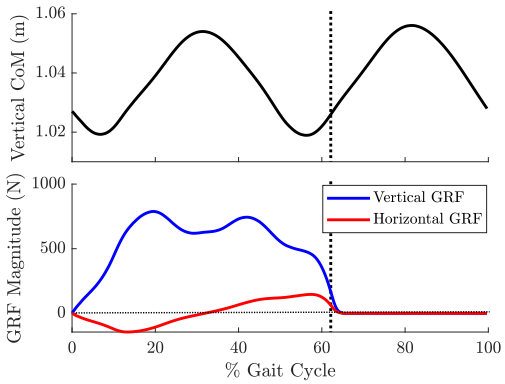

Fig. 3. Vertical CoM and GRF reference tapes from the optimization framework outlined in [25]. Vertical line corresponds to toe-off (∼63%).

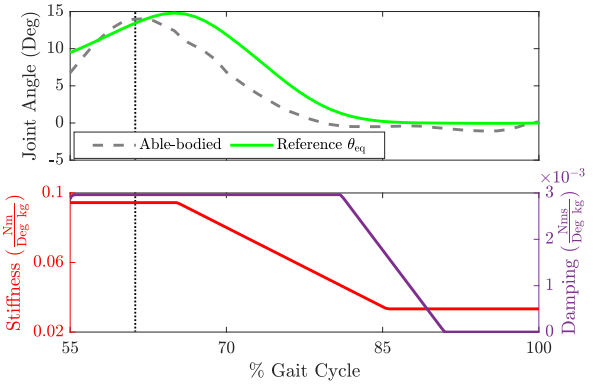

Fig. 4. Impedance parameters for the ankle based on gait cycle progression. Vertical dashed line corresponds to toe-off (∼63%).

were not used in the current work. However, this additional information could be explored in future implementations to address inevitable stride-to-stride variability in the gait [26].

C. Task-space Controller

The controller was comprised of a stance phase, where TSC was active, and a swing phase, which followed a continuous impedance control law. The architectures are discussed in more detail below.

1) Stance Controller: The stance controller featured a feedforward and feedback component, as highlighted in Fig. 2. The feedforward component converted the reference GRF trajectories from Sec. II-B into joint torques via the Jacobian $\mathbf{J}$ of a three-link model of the leg. The link lengths matched the measured lengths of the thigh, shank, and foot of the subject, while the orientation of each link was based on real-time joint kinematics measured via motion capture. The feedforward torque $\boldsymbol{\tau}_{\mathrm{FF}}$ was then calculated as

$$\boldsymbol{\tau}_{\mathrm{FF}} = \mathbf{J}^{\top}\mathbf{F} - \mathbf{D}_{\mathrm{FF}}\dot{\boldsymbol{\theta}} \tag{3}$$

where $\mathbf{F}$ is the reference GRFs, $\dot{\boldsymbol{\theta}}$ is the joint velocity, and $\mathbf{D}_{\mathrm{FF}}$ is a damping gain to discourage sudden joint movements particularly in early stance. The value for $\mathbf{D}_{\mathrm{FF}}$ varied between 0.067 and 0.191 $\frac{\mathrm{Nms}}{\mathrm{Deg}}$ depending on the variable transmission ratio from the four-bar mechanism in the ankle joint. The reference GRFs act at the center of pressure (CoP) of the foot, which was assumed to progress linearly from heel to toe during the stance phase. Note that this formulation can calculate $\boldsymbol{\tau}_{\mathrm{FF}}$ for ankle and knee-ankle control, however ankle-only was the focus of this work.

The feedback torque $\boldsymbol{\tau}_{\mathrm{FB}}$ used the reference CoM trajectories from Sec. II-B with real-time CoM kinematics as a force correction that may be needed to address balance disturbances. The value for $\boldsymbol{\tau}_{\mathrm{FB}}$ was determined using

$$\begin{aligned} \boldsymbol{\tau}_{\mathrm{FB}} &= \mathbf{J}^{\top}\mathbf{K}_{\mathrm{FB}}\boldsymbol{\Delta}_{\mathrm{com}} \\ \mathbf{K}_{\mathrm{FB}} &= \mathrm{diag}(\boldsymbol{\alpha})^{-1}\frac{mg}{H} \end{aligned} \tag{4}$$

where $\boldsymbol{\Delta}_{\mathrm{com}}$ is the discrepancy between reference CoM and real-time CoM information, $\mathbf{K}_{\mathrm{FB}}$ is the feedback gain, m and H are the mass and height of the subject, g is gravity, and $\boldsymbol{\alpha} = [10, 0.02]$ are tuning parameters for the fore/aft and vertical direction, respectively. The commanded stance torque $\boldsymbol{\tau}_{\mathrm{st}}$ was then $\boldsymbol{\tau}_{\mathrm{st}} = \boldsymbol{\tau}_{\mathrm{FF}} + \boldsymbol{\tau}_{\mathrm{FB}}$.

2) Swing Controller: The methods used for the stance controller cannot be applied without GRFs. Therefore, a continuous impedance controller was employed for swing as detailed in [27]. The equilibrium angle θ_{eq}, stiffness k_{eq}, and damping b_{eq} for impedance control are shown in Fig. 4 with respect to the gait cycle. The commanded torque $\boldsymbol{\tau}_{\mathrm{sw}}$ was

$$\boldsymbol{\tau}_{\mathrm{sw}} = -k_{\mathrm{eq}}(\theta - \theta_{\mathrm{eq}}) - b_{\mathrm{eq}}\dot{\theta} \tag{5}$$

where θ is the measured joint angle.

To ensure a smooth transition from stance to swing, a weighted average of $\boldsymbol{\tau}_{\mathrm{st}}$ and $\boldsymbol{\tau}_{\mathrm{sw}}$ was used as the overall commanded torque during the last 7.5% of stance. This weighted average $\boldsymbol{\tau}^{*}$ was determined using

$$\begin{aligned} \boldsymbol{\tau}^{*} &= C_1\boldsymbol{\tau}_{\mathrm{sw}} + (1 - C_1)\boldsymbol{\tau}_{\mathrm{st}} \\ C_1 &= \max\left(\min\left(\frac{\gamma_{\mathrm{est}} - \gamma_{\mathrm{st}} + 7.5\%}{7.5\%}, 1\right), 0\right) \end{aligned} \tag{6}$$

where C_1 is the weight factor, γ_{est} is the estimated progression through the gait cycle, and γ_{st} is the duration of the gait cycle that is spent in stance (∼63%).

D. Phase Estimation

With both the task-space reference parameters and the controller defined with respect to gait cycle progression, accurate real-time gait progression estimation was required for the controller. Visualized in Fig. 5, gait cycle progression was estimated based on the relationship between global tibia angular displacement θ_{tib} and velocity $\dot{\theta}_{\mathrm{tib}}$ in the sagittal plane [19]. The phase variable ϕ was the angle made between the positive x-axis and the line drawn from the origin to any point along the curve. The value of ϕ must change monotonically along the curve, which was ensured by shifting $(\theta_0, \dot{\theta}_0)$ and scaling (k) θ_{tib} and $\dot{\theta}_{\mathrm{tib}}$ using

$$\begin{aligned} \theta^{*}_{\mathrm{tib}} &= \theta_{\mathrm{tib}} - \theta_0 \\ \dot{\theta}^{*}_{\mathrm{tib}} &= k(\dot{\theta}_{\mathrm{tib}} - \dot{\theta}_0) \end{aligned} \tag{7}$$

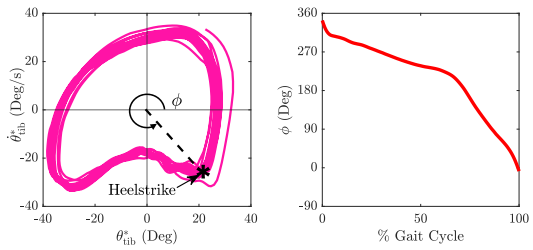

Fig. 5. Phase portrait for global tibia angle and angular velocity after Critical Point Centering [20] with resulting monotonic phase variable.

such that the point of maximum tibia velocity during stance was aligned vertically with the origin, and the range of θ^*_{tib} and $\dot{\theta}^*_{\text{tib}}$ were approximately equal, known as Critical Point Centering [20]. The phase angle was then calculated as $\phi = \text{atan2}(\dot{\theta}^*_{\text{tib}}, \theta^*_{\text{tib}})$.

III. Experimental Setup

A. Hardware

The controller presented here was implemented on the Open-Source Leg (OSL) V1 [28], which was actuated by a Dephy ActPack motor V0.2B [29]. An XSENS MVN Link inertial motion capture suit provided real-time kinematics at a maximum frequency of 240Hz using the lower-body plus sternum configuration [30]. Contact sensing was accomplished via two pressure sensors (SEN-08685; SparkFun Electronics) located at the heel and toe of the prosthetic foot. Data reception and code was conducted on a Raspberry Pi 4 microcomputer. The pressure sensors and motor were wired directly to the Pi, while XSENS data was wirelessly streamed over IP and UDP protocol on a private network using the XSENS Analyze software. The controller and real-time kinematics experimentally ran at ∼210Hz, while data for post-trial analysis was collected at ∼105Hz (see Sec. IV). This initial implementation was performed with an able-bodied subject who donned a bypass adapter for the ankle-only configuration of the OSL (Fig. 1).

B. Calibration Process

The XSENS suit was calibrated first to ensure accurate kinematic estimation. This involved the user donning the XSENS suit while attached to the prosthesis (Fig. 1) and following the standard calibration procedure provided within the XSENS Analyze software. The prosthesis was set to a passive control mode that mimics the functionality of a passive device (Table I).

The phase variable parameters were then calibrated. After finding the subject's PWS on the treadmill, the user treadmill walked for 30 seconds to log CoM and joint kinematics with the prosthesis in passive mode. The joint kinematic data was used offline to calculate θ_0, $\dot{\theta}_0$, and k for reliable gait estimation, while the CoM kinematic data was used for scaling the normalized CoM trajectories from Sec. II-B to generate the reference CoM and GRF profiles.

TABLE I
Finite-State and Passive Impedance Parameters

	Passive	Finite-State		
Parameter		Early Stance	Late Stance	Swing
θ_{eq} (Deg)	0	-1	12	0
k_{eq} ($\frac{\text{Nm}}{\text{Deg kg}}$)	0.10	0.08	0.08	0.05
b_{eq} ($\frac{\text{Nms}}{\text{Deg kg}}$)	0.08	0.02	0.06	0.06

IV. Results

Initial ankle-only implementation was conducted with an able-bodied individual (male, 27 yrs. old, 181.6 cm, 77.1 kg) using a bypass adapter (Fig. 1). After a brief acclimation period and calibration, the user performed four 1-minute treadmill trials at their PWS (0.9 m/s), with time for rest between trials. Trials one and two were run with the ankle in passive mode and an FSM controller [8], respectively, with pertinent parameters provided in Table I. Trials three and four used TSC, without and with CoM feedback (TSC_0, TSC_1), respectively. A minimum of 40 continuous steady-state strides were recorded for each trial.

The following data was logged for post-trial analysis. The XSENS data stream was logged for real-time CoM and segment kinematics, while the onboard sensors of the motor were recorded for joint position/velocity information, as well as motor current data to determine joint torque. Online calculations of information such as $\boldsymbol{\tau}_{\text{FF}}$, $\boldsymbol{\tau}_{\text{FB}}$, and γ_{est} were also recorded for post-trial analysis. During post-trial analysis, data was separated into different gait cycles based on γ_{est} before calculating the average and standard deviation across the gait cycle. All data is reported with respect to the average gait cycle.

Statistical analysis looked at the residual between real-time vertical CoM and reference vertical CoM trajectory for each controller. After calculating the absolute residual between real-time and reference vertical CoM at each time step and separating the data into individual gait cycles for each controller, the data was then binned every 9% of gait cycle, for a total of 11 bins. This breakdown was chosen to align with the transition between stance and swing (∼63%). A type two one-way ANOVA was conducted for each bin, with $p \leq 0.01$ considered significant for all post-hoc pairwise t-tests. A Bonferroni correction using $p \leq 0.0009$ was applied in the same methodology as [31] to mitigate Type I errors. All post-trial analysis was completed in Matlab 2020b. Note that this statistical analysis was not conducted for the joint-level characteristics because there is no joint-level reference trajectory used. Rather, the normative joint-level trajectories are used for qualitative comparisons.

Fig. 6 illustrates the average CoM kinematics with respect to the gait cycle. All trajectories were qualitatively similar to the reference. The average residual $e_{\text{CoM,avg}}$ (mean±st. dev.) between real-time vertical CoM and reference vertical CoM for each controller is provided in Table II. The difference of means with lower and upper bounds between the passive controller and the three other controllers for each bin is illustrated in Fig. 7. The solid markers denote statistically

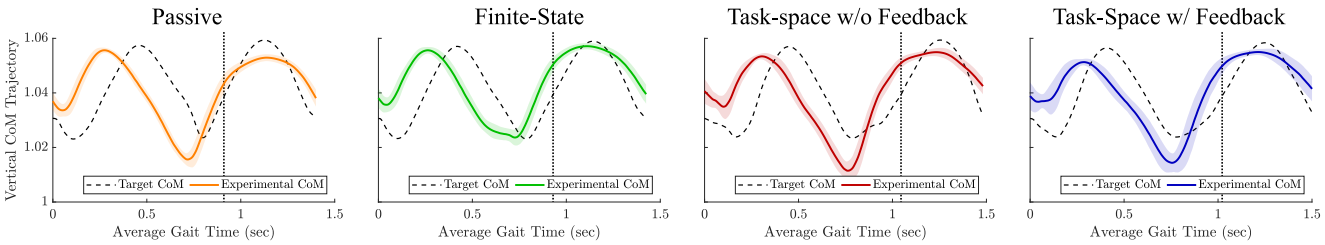

Fig. 6. Mean and standard deviation for the center of mass vertical trajectory with respect to time normalized over a gait cycle. From left to right, the columns correspond to control using passive, finite-state, task-space without feedback, and task-space with feedback. Vertical dashed line denotes toe-off.

TABLE II
CONTROLLER PERFORMANCE

	Control Mode			
Metric	Passive	FSM	TSC_0	TSC_1
e_{CoM} (m)	0.0107 $\pm$0.007	0.0099 $\pm$0.005	0.0102 $\pm$0.005	0.0092 $\pm$0.004
τ_{max} ($\frac{Nm}{kg}$)	0.927	1.366	0.926	1.128
P_{max} ($\frac{W}{kg}$)	0.758	1.745	1.592	1.479

significant difference of means based on the post-hoc pairwise t-tests.

Fig. 8 shows the average desired ankle torque for TSC_0 and TSC_1 based on Equations 3 and 4, while Fig. 9 shows the average ankle kinematics and kinetics with respect to normative data from [23] over the gait cycle. The normative data was scaled to reflect that the OSL has only $\pm 15°$ in dorsi- and plantar flexion. While the passive controller did not produce any plantarflexion, the active controllers qualitatively aligned with desired joint kinematics including plantarflexion.

All control modes produced torque and power profiles qualitatively similar to normative data. Peak torque and power output (τ_{max} and P_{max}, respectively) for each controller are provided in Table II. Power was calculated by multiplying the torque with the joint velocity at each time instant. The peak power tended to occur later than seen in the normative data.

V. DISCUSSION

While TSC_0 and TSC_1 used task-space information to generate desired torques, the resulting joint trajectories of the prosthesis consequently show very good qualitative matching with normative data as well. This result aligns with [14] where task-space kinematic feedback reproduced joint-level muscle activations. All active controllers demonstrate some increased variation in joint-level characteristics compared to the passive controller, however the subject did not report any perceived significant changes in step-to-step controller performance.

All active controllers achieve plantarflexion during late stance that is not achieved by the passive controller. A secondary plantarflexion peak occurs early in the swing phase for TSC_0 that may increase risk of foot-scuffing, however this characteristic appears to be mitigated in TSC_1. This secondary peak may be due to some interaction effects when meshing the stance and swing controllers. Even without CoM feedback, the feedforward torque from the reference GRF trajectories produced joint torque profiles that qualitatively match normative profiles. While TSC_0 did not produce a higher peak ankle torque compared to the passive controller, the ability to generate a plantarflexion angle yielded a higher peak ankle power compared to the passive controller. Incorporating CoM feedback in TSC_1 generated both increased peak ankle torque and power compared to the passive controller.

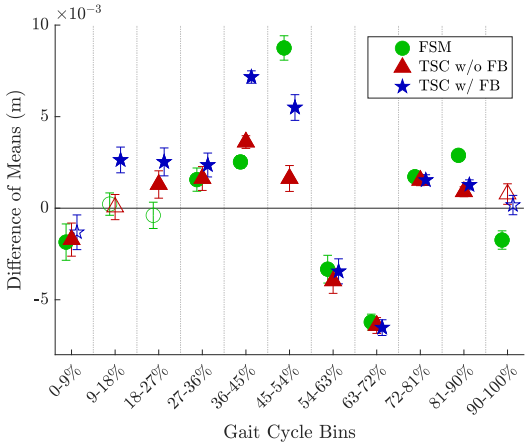

Fig. 7. Difference of means with upper and lower bounds between the passive controller and each of the other controllers. Solid markers denote statistically significant results ($p \leq 0.0009$ with Bonferroni correction).

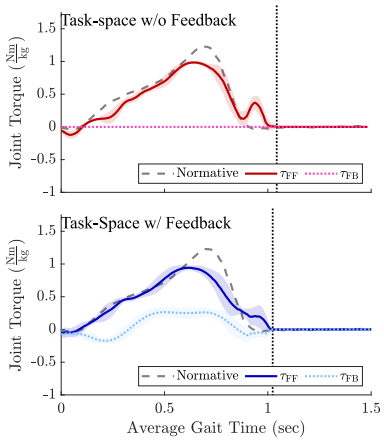

Fig. 8. Mean and standard deviation τ_{FF} and τ_{FB} for task-space control modes. Vertical dashed line denotes the stance-to-swing transition.

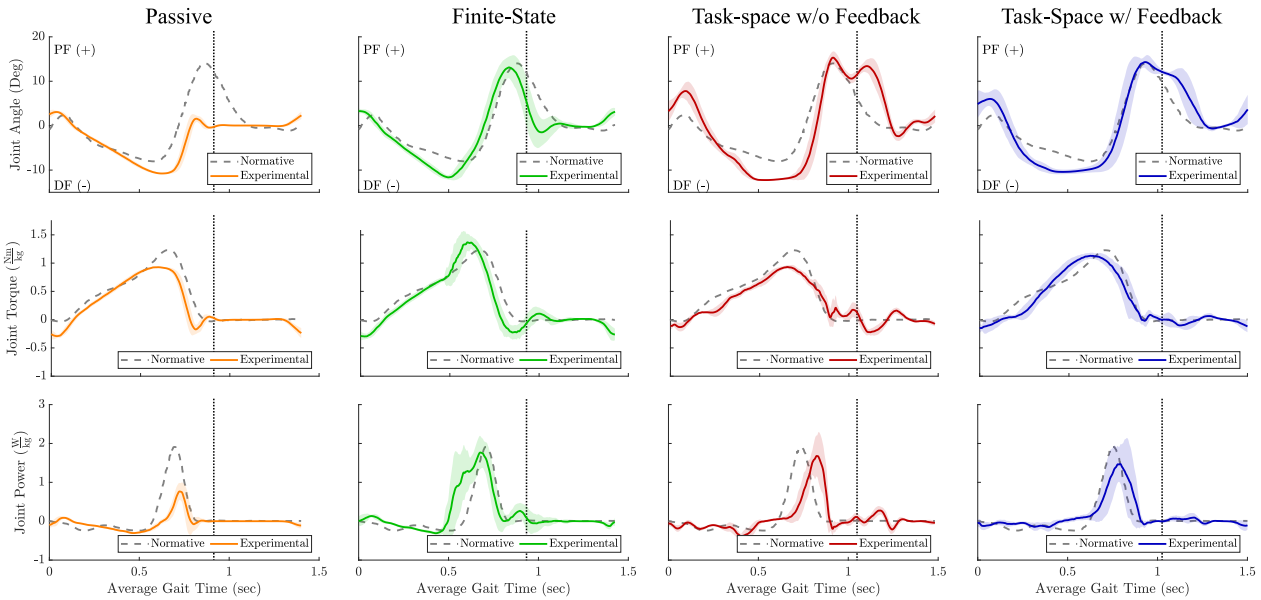

Fig. 9. Mean and standard deviation for the ankle displacement, normalized torque, and normalized power of the prothesis with respect to average gait cycle time. From left to right, the columns correspond to control using passive, finite-state, task-space without feedback, and task-space with feedback. Normative trajectories are adapted from [23]. Vertical dashed line denotes stance-to-swing transition.

Looking at the statistical comparisons, while all active controllers reduced the error in tracking the reference CoM compared to the passive controller, TSC_1 resulted in the overall lowest error. Breaking down by bins, the passive controller showed better CoM tracking at the transition points between stance and swing compared to the active controllers. This may be due to impacts on vertical CoM from the changes in control parameters and methodology at these transition points for the active controllers. For the majority of the stance phase, all active controllers statistically improved CoM tracking. For 9%-54% of the stance phase, TSC_1 had the best improvement in CoM tracking for all but one bin, highlighting the impact of incorporating CoM feedback. Even during the swing phase when TSC is not active, the active controllers were able to improve CoM tracking. This improvement may be due to the ability to produce plantarflexion and help elevate the vertical displacement of the CoM to more closely align with the reference trajectory. The reduced vertical CoM symmetry across controllers compared to the reference trajectory may be due in part to the change in biomechanics from walking with the increased weight of the prosthesis and bypass adapter.

The authors are optimistic that the general framework presents low barrier to application across individuals. This framework requires accurate segment and CoM kinematics data that is robust to interference and latency. A protocol for consistent calibration of the XSENS suit has been developed to accomplish this to mitigate electromagnetic interference from the actuator. While the ankle-only configuration for the OSL was presented here, the framework can be extended to knee-ankle control. Simulated knee torques generated while running the task-space controller for the ankle suggest that the framework can extend to knee-ankle control with proper feedback implementation (Fig. 10).

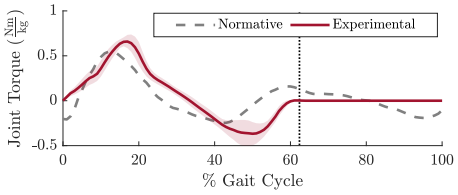

Fig. 10. Simulated knee torque while controlling the ankle-only prosthesis. Normative trajectory is adapted from [23]. Vertical line denotes toe-off.

Overall, it is emphasized that the controller did not target joint-level tracking performance during stance, instead focusing on the CoM. The fact that the joint-level trajectories match normative data brings further support to previous evidence that joint-level trajectories seen in people without amputation may be the by-product of other mechanisms of whole-body coordination, and not the end goal themselves. Future work will further consider how this new perspective on coordinating the user and their prosthesis through the CoM may influence balance beyond steady-state walking.

VI. Conclusion

To conclude, this work presented an initial implementation of task-space control for an ankle-only prosthesis with an able-bodied subject at preferred walking speed. Reference CoM kinematic and GRF profiles were used to calculate desired torques during the stance phase. Results demonstrate that the controller produced ankle kinematic and kinetic profiles that show qualitatively good matching to able-bodied profiles. Future work is focused on expanding the controller beyond preferred walking speed and level-ground, as well as extending the control framework to knee-ankle prostheses.

REFERENCES

[1] W. C. Miller, M. Speechley, and B. Deathe, "The prevalence and risk factors of falling and fear of falling among lower extremity amputees," *Archives of physical medicine and rehabilitation*, vol. 82, no. 8, pp. 1031–1037, 2001.

[2] M. R. Tucker, J. Olivier, A. Pagel, H. Bleuler, M. Bouri, O. Lambercy *et al.*, "Control strategies for active lower extremity prosthetics and orthotics: a review," *Journal of neuroengineering and rehabilitation*, vol. 12, no. 1, pp. 1–30, 2015.

[3] T. Lenzi, M. Cempini, L. Hargrove, and T. Kuiken, "Design, development, and testing of a lightweight hybrid robotic knee prosthesis," *The International Journal of Robotics Research*, vol. 37, no. 8, pp. 953–976, 2018.

[4] Y. Feng, J. Mai, S. K. Agrawal, and Q. Wang, "Energy regeneration from electromagnetic induction by human dynamics for lower extremity robotic prostheses," *IEEE Transactions on Robotics*, vol. 36, no. 5, pp. 1442–1451, 2020.

[5] S. Rezazadeh, D. Quintero, N. Divekar, E. Reznick, L. Gray, and R. D. Gregg, "A phase variable approach for improved rhythmic and non-rhythmic control of a powered knee-ankle prosthesis," *IEEE Access*, vol. 7, pp. 109 840–109 855, 2019.

[6] T. K. Best, K. R. Embry, E. J. Rouse, and R. D. Gregg, "Phase-variable control of a powered knee-ankle prosthesis over continuously varying speeds and inclines," in *2021 IEEE International Conference on Intelligent Robots and Systems (IROS)*. IEEE, 2021, pp. 6182–6189.

[7] C. Ferreira, L. P. Reis, and C. P. Santos, "Review of control strategies for lower limb prostheses," in *Robot 2015: Second Iberian Robotics Conference*. Springer, 2016, pp. 209–220.

[8] F. Sup, H. A. Varol, and M. Goldfarb, "Upslope walking with a powered knee and ankle prosthesis: initial results with an amputee subject," *IEEE transactions on neural systems and rehabilitation engineering*, vol. 19, no. 1, pp. 71–78, 2010.

[9] T. K. Best, C. G. Welker, E. J. Rouse, and R. D. Gregg, "Data-driven variable impedance control of a powered knee–ankle prosthesis for adaptive speed and incline walking," *IEEE Transactions on Robotics*, 2023.

[10] N. Thatte and H. Geyer, "Toward balance recovery with leg prostheses using neuromuscular model control," *IEEE Transactions on Biomedical Engineering*, vol. 63, no. 5, pp. 904–913, 2015.

[11] J. Mendez, S. Hood, A. Gunnel, and T. Lenzi, "Powered knee and ankle prosthesis with indirect volitional swing control enables level-ground walking and crossing over obstacles," *Science Robotics*, vol. 5, no. 44, p. eaba6635, 2020.

[12] V. Lugade, V. Lin, and L.-S. Chou, "Center of mass and base of support interaction during gait," *Gait & posture*, vol. 33, no. 3, pp. 406–411, 2011.

[13] A. L. Hof, M. Gazendam, and W. Sinke, "The condition for dynamic stability," *Journal of biomechanics*, vol. 38, no. 1, pp. 1–8, 2005.

[14] S. A. Safavynia and L. H. Ting, "Long-latency muscle activity reflects continuous, delayed sensorimotor feedback of task-level and not joint-level error," *Journal of neurophysiology*, vol. 110, no. 6, pp. 1278–1290, 2013.

[15] S. Kajita, F. Kanehiro, K. Kaneko, K. Yokoi, and H. Hirukawa, "The 3d linear inverted pendulum mode: A simple modeling for a biped walking pattern generation," in *Proceedings 2001 IEEE International Conference on Intelligent Robots and Systems. Expanding the Societal Role of Robotics in the the Next Millennium (Cat. No. 01CH37180)*, vol. 1, 2001, pp. 239–246.

[16] S. Kuindersma, R. Deits, M. Fallon, A. Valenzuela, H. Dai, F. Permenter, T. Koolen, P. Marion, and R. Tedrake, "Optimization-based locomotion planning, estimation, and control design for the atlas humanoid robot," *Autonomous robots*, vol. 40, pp. 429–455, 2016.

[17] Y. Liu, P. M. Wensing, D. E. Orin, and Y. F. Zheng, "Trajectory generation for dynamic walking in a humanoid over uneven terrain using a 3d-actuated dual-slip model," in *IEEE International Conference on Intelligent Robots and Systems (IROS)*, 2015, pp. 374–380.

[18] J. Pratt, J. Carff, S. Drakunov, and A. Goswami, "Capture point: A step toward humanoid push recovery," in *2006 6th IEEE-RAS international conference on humanoid robots*. IEEE, 2006, pp. 200–207.

[19] M. A. Holgate, T. G. Sugar, and A. W. Bohler, "A novel control algorithm for wearable robotics using phase plane invariants," in *2009 IEEE International Conference on Robotics and Automation*. IEEE, 2009, pp. 3845–3850.

[20] R. R. Posh, J. A. Tittle, J. P. Schmiedeler, and P. M. Wensing, "Calibration of a tibia-based phase variable for control of robotic transtibial prostheses," in *IEEE International Conference on Intelligent Robots and Systems*, 2023, pp. 1–6.

[21] C. Ochoa-Diaz and A. Padilha L. Bó, "Symmetry analysis of amputee gait based on body center of mass trajectory and discrete fourier transform," *Sensors*, vol. 20, no. 8, p. 2392, 2020.

[22] M. Schaarschmidt, S. W. Lipfert, C. Meier-Gratz, H.-C. Scholle, and A. Seyfarth, "Functional gait asymmetry of unilateral transfemoral amputees," *Human movement science*, vol. 31, no. 4, pp. 907–917, 2012.

[23] D. A. Winter, "Biomechanical motor patterns in normal walking," *Journal of motor behavior*, vol. 15, no. 4, pp. 302–330, 1983.

[24] C. A. Fukuchi, R. K. Fukuchi, and M. Duarte, "A public dataset of overground and treadmill walking kinematics and kinetics in healthy individuals," *PeerJ*, vol. 6, p. e4640, 2018.

[25] D. J. Kelly and P. M. Wensing, "Optimizing template models to quantifiably assess center of mass kinematic reconstruction," in *2022 International Conference on Rehabilitation Robotics (ICORR)*. IEEE, 2022, pp. 1–6.

[26] S. X. Yang, P. K. Larsen, T. Alkjær, E. B. Simonsen, and N. Lynnerup, "Variability and similarity of gait as evaluated by joint angles: implications for forensic gait analysis," *Journal of forensic sciences*, vol. 59, no. 2, pp. 494–504, 2014.

[27] R. R. Posh, J. A. Tittle, D. J. Kelly, J. P. Schmiedeler, and P. M. Wensing, "Hybrid volitional control of a robotic transtibial prosthesis using a phase variable impedance controller," in *IEEE International Conference on Robotics and Automation (to appear)*, 2024.

[28] A. F. Azocar, L. M. Mooney, J.-F. Duval, A. M. Simon, L. J. Hargrove, and E. J. Rouse, "Design and clinical implementation of an open-source bionic leg," *Nature biomedical engineering*, vol. 4, no. 10, pp. 941–953, 2020.

[29] J.-F. Duval and H. M. Herr, "Flexsea: flexible, scalable electronics architecture for wearable robotic applications," in *2016 6th IEEE International Conference on Biomedical Robotics and Biomechatronics (BioRob)*. IEEE, 2016, pp. 1236–1241.

[30] D. Roetenberg, H. Luinge, P. Slycke *et al.*, "Xsens mvn: Full 6dof human motion tracking using miniature inertial sensors," *Xsens Motion Technologies BV, Tech. Rep*, vol. 1, pp. 1–7, 2009.

[31] T. M. Gambon, J. P. Schmiedeler, and P. M. Wensing, "Effects of user intent changes on onboard sensor measurements during exoskeleton-assisted walking," *IEEE Access*, vol. 8, pp. 224 071–224 082, 2020.